NJC

ROYAL SOCIETY OF CHEMISTRY

PAPER

View Article Online
View Journal

Cite this: DOI: 10.1039/d3nj04662a

Weakly antiferromagnetic vanillin and acetate bridged dinuclear Ni(II) compound exhibiting catecholase-like activity and biological properties†

Beena K. Vernekar, *[ab] Nikita N. Harmalkar,[a] Sanket K. Gaonkar,[c] Jhuma Sannigrahi[d] and Sunder N. Dhuri *[a]

Received 6th October 2023,
Accepted 15th January 2024

DOI: 10.1039/d3nj04662a

rsc.li/njc

A dinuclear nickel compound that features vanillin (van) and acetate (OAc) bridging ligands, $[Ni_2(\mu\text{-van})_2(\mu\text{-OAc})(NCS)_3(H_2O)]\cdot 5H_2O$ **1**, was synthesized and characterized using various techniques. Crystal structure analysis revealed a pair of Ni(II) ions bridged by an acetate anion through a μ_2-η^1:η^1 coordination mode. At the same time, vanillin bridges both nickel(II) centers through phenolic oxygen, separating the two Ni ions by a distance of 3.001(7) Å. The temperature-dependent magnetism indicates weak antiferromagnetic behaviour in compound **1**, following the Curie–Weiss law with Curie constant C = 1.0145 cm^3 K mol^{-1} and Weiss constant θ = −4.1 K. Compound **1** was evaluated for its ability to mimic the catechol oxidase enzyme using 3,5-di-*tert*-butylcatechol as a model substrate with a K_{cat} value of 157.1 × 10^2 h^{-1}. Furthermore, compound **1** was tested for its cytotoxicity against HepG2 cancer cells and DNA cleavage properties.

1. Introduction

The nickel(II) ion presents versatile coordination chemistry due to its inherent ability to adopt various geometries. For many decades, nickel was not thought to be involved in biological processes. Later, the discovery of urease by Zermer in 1975,[1,2] to possess nickel in its active center, was a game changer and served as an initial impetus for bioinorganic chemists to understand significant roles played by Ni(II) in biological metabolism. In many enzymes, such as *E. coli* glyoxalase-I and superoxide dismutase, its functional utility is transparently visible.[3–5] The nickel(II) ion plays a vital role in metalloproteins like hydrogenases, such as carbon monoxide dehydrogenase and acetyl-CoA synthase.[6,7] These enzymes have the ability to activate molecular oxygen at ambient temperatures, and thus there has been a significant focus on nickel(II) enzymes in the past.[8–10] Nickel(II) compounds serving as functional models have been utilized as competent catalysts for several synthetic transformations of industrial importance.[11,12] Metalloenzyme models with oxidase activity have attracted many researchers, in the pursuit of creating bio-inspired catalysts for organic oxidation.[13]

Nickel(II) has been implicated in the pathogenesis of certain diseases: for example, nickel(II) ions can interact with proteins and induce immune responses in individuals who are allergic to nickel.[14] Furthermore, a plethora of nickel(II) compounds with biological activities, such as anti-tumor antibiotics,[15] anticonvulsants, antiepileptic drugs, or vitamins, have been reported.[16–18] In an attempt to evaluate nickel(II) compounds biologically, many of them that exhibit noteworthy potential as antibacterial and anti-fungal agents,[19–21] as well as those that show anti-inflammatory[22] and antioxidant[23–25] activity, have been explored and verified. Additionally, various nickel(II) compounds have been reported to act as DNA intercalators[26,27] and DNA cleavage agents.[28,29] These compounds possess effective anti-proliferative activity towards diverse cell lines and have been adequately substantiated in the literature.[30–32]

Dinuclear transition metal compounds play prominent roles in electron transfer processes in metallobiomolecules,[33–37] which can be confirmed by citing an example of a unique representation of a heteroleptic paddlewheel complex of nickel(II) that has been synthesized and structurally characterized.[38] Extensive research has been dedicated to the

[a] School of Chemical Sciences, Goa University, Taleigao Plateau, Goa, 403206, India. E-mail: sndhuri@unigoa.ac.in, beena.vernekar@khandolacollege.edu.in
[b] Department of Chemistry, Government College of Arts, Science and Commerce, Khandola, Marcela, Goa, 403107, India
[c] Department of Microbiology, P.E.S's R.S.N College of Arts, and Science, Farmagudi, Ponda, Goa, 403401, India
[d] School of Physical Sciences, Indian Institute of Technology, Farmagudi, Ponda, Goa, 403401, India

† Electronic supplementary information (ESI) available. CCDC 2285723. For ESI and crystallographic data in CIF or other electronic format see DOI: https://doi.org/10.1039/d3nj04662a

synthesis of dinuclear metal compounds that mimic several metallobiomolecules like urease[39–41] and catecholase.[42–44] Dinuclear nickel(II) compounds have been known to catalyze catechol oxidation.[45,46] The ligating groups play indispensable roles in establishing a linkage between the biological function and relevance of the compound. A well-known and multifaceted ligand studied in large applications is *p*-vanillin (4-hydroxy-3-methoxybenzaldehyde), which occurs naturally in various plants. It is synthetically obtained as a by-product of the sulfite process in the manufacture of wood pulp.[47] *p*-vanillin is commonly used as a flavouring or fragrance agent in food items, perfumes, beverages, cosmetics, and the pharmaceutical industry.[48] *p*-Vanillin exhibits non-linear properties with second harmonic generation efficiency, and thus, it has potential for use in the fabrication of optical devices.[49]

Apart from its industrial and economic value, *p*-vanillin has been effectively authenticated as a significant bioactive substance. It is an effective anti-mutagenic agent and reduces certain species that induce mutations in bacteria and subsequently inhibits spontaneous mutations.[50] The bioactivity of *p*-vanillin is propagated through the fact that it can significantly reduce mutations caused by ultraviolet light and X-rays in mammalian cells and hamster lung cells (V79).[51] The innate ability of *p*-vanillin to cause DNA cleavage and its ability to induce the apoptosis of HepG2 cancer cells were very well supported in our recent study.[52] Our up-to-date search of the CSD provided us with a few structures of transition metal complexes incorporating *p*-vanillin[53–56] and a single mononuclear compound has been specifically reported for nickel.[57] Considering the importance of *p*-vanillin in biology and scarcity of studies on nickel-vanillin compounds, we herein report the structural, spectroscopic, and magnetic properties of a new dinuclear nickel(II)-vanillin compound **1** with subordinate acetate and isothiocyanate ligands. The catecholase-like activity of the dinuclear compound is demonstrated along with a presentation of the efficacy of compound **1** in cytotoxicity studies and DNA cleavage.

2. Experimental section

2.1. Materials and methods

The chemicals used in this study were procured from local chemical vendors and used as received without further purification or recrystallization. Infrared spectra of powdered compound **1** and associated ligands were measured on a Shimadzu FTIR spectrophotometer (IR-Prestige-21) in the region 4000–400 cm^{-1} at 4 cm^{-1} resolution in a KBr matrix. UV-Vis absorption spectra were recorded on a diode array photocathode Agilent UV-Vis spectrophotometer (model-8453). Elemental analyses were achieved using an Elementar Vario MACRO cube CHNS analyzer. Powder X-ray diffraction (PXRD) data were collected on a Bruker D8 Advance X-ray diffractometer using Cu $K\alpha_1$ (λ = 1.5406 Å) with an Ni filter. Temperature-dependent magnetic measurements of polycrystalline sample **1** were carried out using a SQUID-VSM MPMS3 magnetometer in the temperature range of 60 to 310 K. The temperature-dependent variation of field-cooled (FC) and zero-field-cooled (ZFC) magnetization (M) was measured with a magnetic field of 100 Oe. The ^{1}H NMR spectra were recorded on a Bruker 500 MHz instrument with tetramethylsilane (TMS) as an internal standard in $CDCl_3$ at IIT Goa.

2.2. Single crystal X-ray diffraction (SCXRD)

The single crystal X-ray structure determination of compound **1** was achieved using a Bruker D8 QUEST ECO X-ray diffractometer equipped with graphite-monochromated MoKα (λ = 0.7107 Å) radiation. The collected frames were integrated, scaled, and merged, and absorption correction was performed using Bruker's APEX 4 program package. The structure of **1** was solved using SHELXS and subsequent refinements were carried out against F^2 using SHELXL-2014.[58] All non-hydrogen atoms were refined anisotropically. The H-atoms of water molecules were located from a difference map, and hydrogens attached to carbon atoms were refined in calculated positions [C–H = 0.93 Å and O–H = 0.85 Å] with $U_{iso}(H) = 1.2\ U_{eq}(C)$ [1.5 for $U_{eq}(O)$] using a riding model. The technical details of data acquisition and selected refinement results for **1** are given in Table 1.

2.3. Synthesis of $[Ni_2(\mu\text{-van})_2(\mu\text{-OAc})(NCS)_3(H_2O)]\cdot 5H_2O$

A methanolic solution (10 mL) of nickel(II) acetate tetrahydrate (1 mmol, 0.249 g) was added dropwise to a methanolic solution (10 mL) of vanillin (2 mmol, 0.304 g) and ammonium thiocyanate (2 mmol 0.152 g). The reaction mixture was stirred for two

Table 1 Crystal parameters and selected refinement details for compound **1**

Empirical formula	$C_{21}H_{31}N_3Ni_2O_{14}S_3$
Formula weight (g $mole^{-1}$)	763.09
Temperature (K)	296(2)
Wavelength (Å)	0.71073
Crystal system	Monoclinic
Space group	$P2_1/c$
Unit cell dimensions (Å/°)	a = 10.637(14) α = 90 b = 22.981(3) β = 106.458(4) c = 14.427(17) γ = 90
Volume ($Å^3$)	3382.4(7)
Z	4
Density (calculated) (Mg m^{-3})	1.498
Absorption coefficient (mm^1)	1.361
F(000)	1576
Crystal size (mm^3)	0.4 × 0.22 × 0.12
2 theta range for data collection (°)	2.184 to 28.364
Index ranges	$-14 \le h \le 14$, $-30 \le k \le 30$, $-16 \le l \le 19$
Reflections collected	49 980
Independent reflections	8412 [R(int) = 0.0479]
Completeness to theta = 25.242° (%)	99.3
Absorption correction	Semi-empirical from equivalents
Refinement method	Full-matrix least-squares on F^2
Data/restraints/parameters	8412/2/420
Goodness-of-fit on F^2	1.031
Final R indices [$I > 2$sigma(I)]	R_1 = 0.0465, wR_2 = 0.1295
R indices (all data)	R_1 = 0.0661, wR_2 = 0.1334
Extinction coefficient	n/a
Largest diff. peak and hole e ($Å^{-3}$)	0.82 and −0.74
CCDC	2285723

hours, and the green-colored solution was then allowed to evaporate slowly. After two weeks, the green-colored crystals were isolated from mother liquor, washed with isopropanol and ether, and air-dried. Yield of **1** is 0.472 g (55%). Anal. calcd for **1**: $C_{21}H_{31}O_{14}N_3S_3Ni_2$ (M.W. = 763.09 g) C, 33.05; H, 4.10; and N, 5.51 Found: C, 33.77; H, 4.21; and N, 5.39. IR (KBr, cm^{-1}): 3207 (br), 2833 (br), 2113, 2058, 1870 (sh), 1665 (sh), 1562 (sh), 1487 (sh), 1282 (sh), 1001 (sh), and 815 (sh). UV-Vis (DMSO) (λ_{max}, nm): 252, 281, 317, 673 and 742.

2.4. Catecholase-like activity

The catecholase-like activity of dinuclear compound **1** was investigated using 3,5-di-*tert*-butylcatechol (3,5-DTBC) as a model substrate. 3,5-DTBC is known to offer a low quinone-catechol reduction potential, making it an ideal substrate for such studies.[59,60] The efficacy of the Ni(II) compound in catalyzing the oxidation of 3,5-DTBC was studied by adding 100 equivalents of 3,5-DTBC to a 10^{-4} M methanolic solution of **1** saturated with oxygen atmosphere. The reaction proceeds with the formation of a new absorption band at 405 nm, which is attributed to the respective quinone with a distinct color change from light green to yellow for a duration of 30 minutes. A blank experiment was conducted without a catalyst, which showed no quinone formation in MeOH for up to 2 h. The kinetics of the oxidation of 3,5-DTBC in the presence of the catalyst was measured by the initial rate method.[61] The dependence of the initial rate on substrate concentration (100–600 eq.) was spectrophotometrically monitored at 405 nm. Compound **1** showed saturation kinetics; hence, the data was treated with the Michaelis–Menten model. The maximum velocity (V_{max}), binding constant (K_M), and rate constant (K_{cat}) were calculated using the Lineweaver–Burk graph. NMR spectroscopy was used to characterize the isolated product after the catalytic study of compound **1** which was identified to be 3,5-DTBQ (Fig. S5, ESI†). ^{1}H NMR (400 MHz, $CDCl_3$): δ = 6.85 (s, 1H), 6.15 (s, 1H), 1.20 (s, 9H), and 1.16 (s, 9H).

2.5. Detection of H_2O_2 in reaction medium

The generation of hydrogen peroxide during the reaction was determined by an iodometric method. The catalytic reaction was carried out as described in the kinetics experiment. After 1 h, to stop further oxidation, the solution was acidified with H_2SO_4 to pH 2. To the acidified solution, 10% KI solution (1 mL) was added, followed by the addition of 3% ammonium molybdate solution to increase the rate of the reaction.[62] 3,5-DTBQ was then extracted twice with CH_2Cl_2 from the reaction medium. The formation of I^{3-} could then be spectrophotometrically monitored using the aqueous layer. In blank experiments under identical conditions, only minor formation of I^{3-} was observed in the presence of just 3,5-DTBC or the catalyst.

2.6 Cytotoxicity studies

The cytotoxic effect of compound **1** was determined by a colorimetric assay that measures the reduction of yellow 3-(4,5-dimethythiazol-2-yl)-2,5-diphenyltetrazolium bromide (MTT) to an insoluble and dark purple formazan product by mitochondrial succinate dehydrogenase of viable cells. HepG2 cell lines were used for this study. The cell lines were cultured in Dulbecco's modified Eagle medium with low glucose (Gibco, Invitrogen) supplemented with 10% foetal bovine serum (FBS) (Gibco, Invitrogen) and antimycotic 100× solution (Thermo Fisher Scientific). The cells were seeded in a 96-well flat-bottom microplate and maintained at 37 °C in 95% humidity and 5% CO_2 overnight. Different concentrations (100, 50, 25, 12.5, 6.25, and 3.125 μg mL^{-1}) of **1** were treated with cells for a duration of 48 hours. The wells were washed twice with PBS; 20 μL of the MTT staining solution was added to each well, and the plate was incubated at 37 °C. After 4 h, 100 μL of DMSO was added to each well to dissolve the formazan crystals, and the absorbance was recorded using a microplate reader at 570 nm. Untreated cells with media and *cis*-platin were maintained as negative and positive controls, respectively. The experiments were carried out in triplicates, and the cell viability relative to untreated cells was determined using eqn (1).

$$\text{Surviving cells (\%)} = \text{mean OD of test compound/mean OD of negative control} \times 100 \quad (1)$$

2.7. DNA cleavage activity

The DNA cleavage activity of compound **1** was determined according to the procedure developed by Banerjee *et al.* with a slight modification.[63] Briefly, a supercoiled pBR322 (200 μg) artificial plasmid DNA was treated with prepared compound **1** (10 μM, 20 μM, 40 μM, and 80 μM) in Tris buffer (5 mM Tris-HCl, 50 mM NaCl, pH ~ 7.2) to yield a total volume of 10 μL and incubated in the dark for 1 h at 37 °C. The reaction was quenched by adding 3 μL of loading buffer, and resulting solutions were loaded on 1% agarose gel. Electrophoresis was carried out at 80 V for 1 h in Tris-acetate-EDTA (TAE) buffer (pH ~ 8.0). The DNA bands were visualized under UV light and the band intensities and fragmentation patterns observed in the absence and presence of the compound. The results were expressed qualitatively based on the appearance of supercoiled (SC) (form I), nicked circular (NC) (form II), and linear (L) (form III) forms of DNA.

3. Results and discussion

3.1. Synthetic protocol of $[Ni_2(\mu\text{-van})_2(\mu\text{-OAc})(NCS)_3(H_2O)]\cdot 5H_2O$

The synthesis of the dinuclear compound **1** was achieved by reacting 1 mole of nickel(II) acetate tetrahydrate, 2 moles of *p*-vanillin, and 2 moles of ammonium thiocyanate in the ratio 1 : 2 : 2 by a slow evaporation method at room temperature. After 2 weeks, the green-colored crystals that had formed were isolated and washed with isopropanol followed by diethyl ether. Single crystals of **1** were subjected to various characterization techniques like spectroscopy, elemental analysis, SCXRD, and powder diffraction. The synthetic approach for compound **1** is shown in Scheme 1.

3.2. Infrared and UV-Vis spectroscopic studies

The IR spectrum of **1** is depicted in Fig. S1, ESI.† A broad band in the range of 3207 cm^{-1} has been attributed to the water molecules in compound **1** and can also be assigned to the

phenolic –OH group, which is characteristic of a free *p*-vanillin moiety and the weak band at 2833 cm^{-1} is due to C–H vibrations.[64,65] The broadening of this band suggests intramolecular H-bonding with phenolic oxygen. Vanillin bound to Ni(II) in a bridged manner exhibited a stretching band at 1665 cm^{-1} assigned to an aldehydic C=O stretching vibration. Several sharp-to-medium vibrations between ~1590^{-1} and 1420 cm^{-1} could be assigned to C–C vibrations, while those at ~1277 cm^{-1} and ~1150 cm^{-1} could be typical signatures for C–N and methoxy functionalities, respectively.[64–66] The characteristic signatures at 1487–1413 cm^{-1} may be attributed to the symmetric stretching of C–O and the methyl group.[67] The presence of a strong absorption band at 2113 cm^{-1} with a shoulder at 2058 cm^{-1} indicates coordination of isothiocyanate (NCS anion) to the two nickel atoms.[68] The electronic spectrum of compound **1** (2 mM) showed a low-intensity broadband in the region of 600–800 nm when recorded in MeOH solvent. These bands are attributed to d–d transitions (inset Fig. S2, ESI†). The molar extinction of bands arising at 673 and 742 nm is 20.3 and 19 mol^{-1} L cm^{-1}, respectively. Upon diluting the solution to 0.1 mM, we could see bands appearing at 252, 281, and 317 nm, which can be assigned to intra-ligand π–π* and n-π* transitions, suggesting the presence of the vanillin moiety in the compound when compared with the spectrum of free vanillin (Fig. S2, ESI†).[69]

3.3. Single crystal structure of 1

The single crystal data of $[Ni_2(\mu\text{-van})_2(\mu\text{-OAc})(NCS)_3(H_2O)]\cdot 5H_2O$ **1** reveals that the compound crystallizes in the centrosymmetric monoclinic crystal system with $P2_1/c$ space group. The asymmetric unit of **1** discloses the presence of two crystallographically independent nickel(II) ions (Ni1 and Ni2) held together by a bridging acetate ligand in a $\mu\text{-}\eta^1{:}\eta^1$ (*syn–syn*) type of coordination mode and phenolic oxygen (O3 and O6) of *p*-vanillin ligands with Ni–Ni separation of 3.001(7) Å. Apart from the bridging ligand, the asymmetric unit also contains three terminal isothiocyanate moieties of which two show a linear and one a bent coordination mode. The asymmetric unit also comprises one coordinated water molecule attached to the Ni1 and five water molecules in the crystal lattice, as shown in Fig. 1. Both the Ni(II) centers adopt the octahedral geometry; however, the coordination environments are significantly different. The octahedron of the Ni1 centre consists of five oxygen and one nitrogen atom forming an {NiO5N} coordination environment

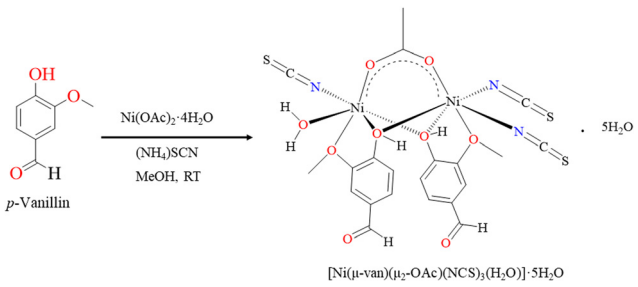

Scheme 1 Preparation of **1** using the above methodology.

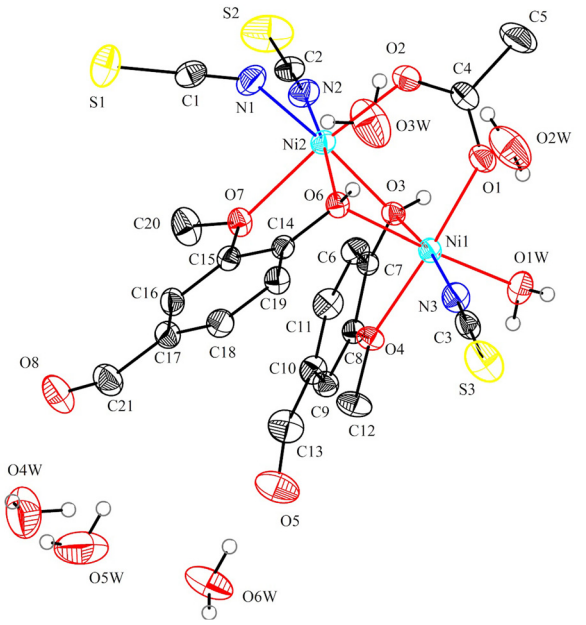

Fig. 1 Asymmetric unit of **1** with atom labelling scheme. The thermal ellipsoids are drawn at a 30% probability level for all non-hydrogen atoms. The hydrogen atoms on the carbon backbone of acetate and *p*-vanillin apart from one on phenolic oxygen have been removed for clarity.

(Fig. S3(left) ESI†). The phenolic oxygen atoms (O3 and O6) occupy two equatorial positions, originating from two-bridging *p*-vanillin, with an average Ni–O bond distance of 2.05 Å. The remaining equatorial sites are occupied by one water molecule (O1W) and one terminal isothiocyanate ligand (N3), adopting linear coordination mode. The Ni–O1W and Ni–N3 bond distances are 2.083(3) and 1.994(3) Å, respectively, agreeing with compounds bearing terminal water and isothiocyanates.[70–72] The axial positions are occupied by two oxygen atoms (O1 and O4) from the bridging acetate and methoxy substituent on the *p*-vanillin ligand, with Ni–O bond distances of 2.031(2) and 2.148(19) Å, respectively, again showing good agreement with related compounds.[73,74] The *cis* N–Ni1–O bond angles range from 92.64(12)° to 95.87(10)°, and the *trans* angle is 171.8°. The *cis* O–Ni1–O bond angles range from 77.11(7)° to 92.13(8)°, with the average *trans* angle being 17°. The deviation from the regular octahedron is discernible from bond distances and bond angles around Ni1.

The Ni2 center in the dinuclear compound also adopts an octahedral coordination, exhibits deviation from a regular octahedron, and tends to form the {NiO4N2} coordination environment depicted in Fig. S3 (right), ESI.† Since *p*-vanillin is involved in bridging, two equatorial sites are occupied by oxygen atoms (O6 and O3), as at the Ni1 center. Moreover, the axial positions here are occupied by two oxygen atoms (O2 and O7) from the bridging acetate and methoxy substituent similar to that in the Ni1 center. The difference lies in the occupancy at equatorial sites, which are now occupied by two nitrogen atoms (N1 and N2), forming the coordination of isothiocyanate ligands. One of the isothiocyanate ligands coordinated through N1 shows bent-type coordination mode, forming a bond angle

of 139.6(3)° for Ni2–N1–C1. Further, the N1 of the isothiocyanate ligand with bent mode forms a slightly longer Ni–N bond 2.057(2) Å compared to the one coordinating *via* the linear isothiocyanate ligand with an average Ni–N bond length of 2 Å. These values are in good agreement with reported compounds with bent and linear isothiocyanate ligands.[75,76] The *cis* N–Ni2–O bond angle ranges from 87.68(11)° to 96.27(10)°, and the average *trans*-N–Ni2–O bond angle is 17°. Selected bond distances and angles are given in Table S1 (ESI†). The bridge mediated by phenolic oxygens between the two Ni centers is asymmetric, as can be seen from varying bond distances between Ni and the phenolic oxygen. The O3 oxygen is attracted more towards the Ni1 center with a bond distance of 2.027(19), whereas the distance from O3 to Ni2 is slightly longer 2.092(2). A similar observation is made for the O6 atom, which lies more towards the Ni2 atom with a bond distance of 2.032(19). This asymmetric type of binding is made possible because of the presence of a methoxy group adjacent to the phenolic oxygen in the *p*-vanillin ligand, which has its oxygen atom coordinating with metal centers. Thus, it can be said that the variation in substituents adjacent to the phenolic oxygen will undoubtedly influence the structural, and therefore, magnetic properties of the material. Moreover, the bridging of the acetate molecule is responsible for the non-planarity of the equatorial base at each Ni(II) site. This results in slight structural folding, with an Ni1–O3–Ni2 bond angle of 93.52(8)° and Ni2–O6–Ni1 of 93.73(8)°.

The geometric parameters of two crystallographically unique *p*-vanillin, acetate, and isothiocyanate ligands are in the normal range as reported in the literature (Table S2, ESI†).[77–79] The hydrogens attached to the coordinated aqua ligand bound to Ni1 of one dinuclear unit function as hydrogen donors, while the S atom of the isothiocyanate ligand coordinated to Ni2 *via* the N atom of the other unit acts as an acceptor, resulting in O1W–H1A···S1 intermolecular hydrogen bonding interactions. The extension of this hydrogen bond along *a*-axes results in a 1D supramolecular chain structure. These 1D chains are then extended along *b*-axes to form a 2D layer structure through hydrogen bonding interaction with the hydrogen atom bonded to the terminal carbon of the acetate group (C5) which acts as a donor atom to the unit in the layer above. The carbonyl oxygen (O8) functions as a hydrogen bond acceptor, thereby interlinking the layers in the *ab* plane, as shown in Fig. 2. These 2D supramolecular layers are further connected through C13–H13···S1 to a 3D hydrogen-bonded network (Fig. 3). The hydrogen bonding parameters of **1** are listed in Table S3 (ESI†).

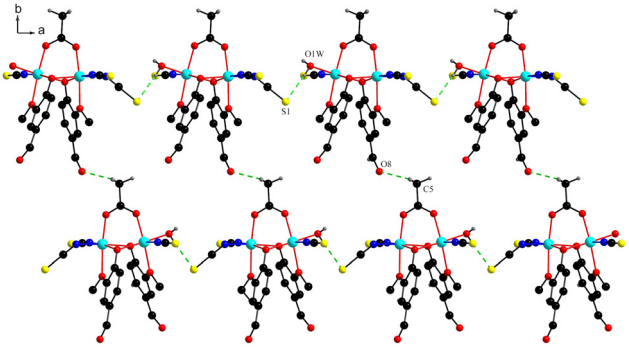

Fig. 2 Intermolecular hydrogen bond O1W–H1A···S1^{i} is responsible for the formation of 1D supramolecular chain assembly along the axes, and the C5–H5A···O8^{ii} bond aids in interlinking the chains into 2D layers along the *ab* plane.

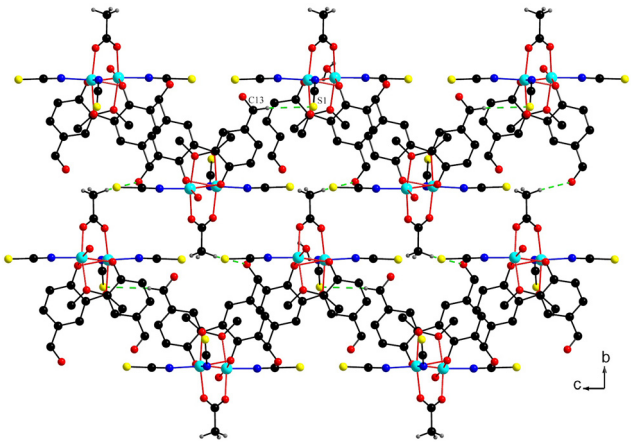

Fig. 3 Further extension of 2D layers along *c*-axes through the C13–H13···S1^{iii} intermolecular hydrogen bond.

3.4. X-ray powder diffraction

The phase purity of the crystalline powder of **1** was determined by comparing the experimental X-ray powder pattern of **1** with its simulated powder pattern obtained using single crystal structure data (Fig. S4, ESI†). The powder patterns closely matched, suggesting that compound **1** is in the pure phase.

3.5. Catechol oxidation by 1

The catechol oxidase enzyme catalyzes the oxidation of various *o*-diphenols to corresponding *o*-quinones.[80] The active site of the enzyme comprises a hydroxo-bridged Cu(II) core wherein copper binds to three histidine nitrogens, forming a trigonal pyramidal structure: a type-3 active site. Due to the advantage of lower redox potential for the quinone-catechol couple, 3,5-di-*tert*-butylcatechol is the most commonly utilized substrate to determine the catalytic potency of a catalyst.[81] To uncover the potential of the titled compound in the oxidation of 3,5-DTBC, we reacted a 1×10^{-4} M methanolic solution of **1** with 1×10^{-2} M (100 equiv.) of 3,5-DTBC. The solvent was saturated with O_2 by bubbling through O_2 gas for about 2 minutes prior to analysis. The course of the reaction was then traced as a function of time with the aid of a UV-Vis spectrophotometer. The time-dependent spectral scans of **1** in the presence of 100 equiv. of substrate are depicted in Fig. 4. From the figure, it is clear that a new band appeared at around 405 nm, the intensity of which increases with time, suggesting the formation of the product in the reaction mixture. To identify the oxidised product, the reaction medium was allowed to evaporate at room temperature, resulting in the formation of dark brown crystals which were isolated and further purified using column chromatography and characterized using NMR spectroscopy in

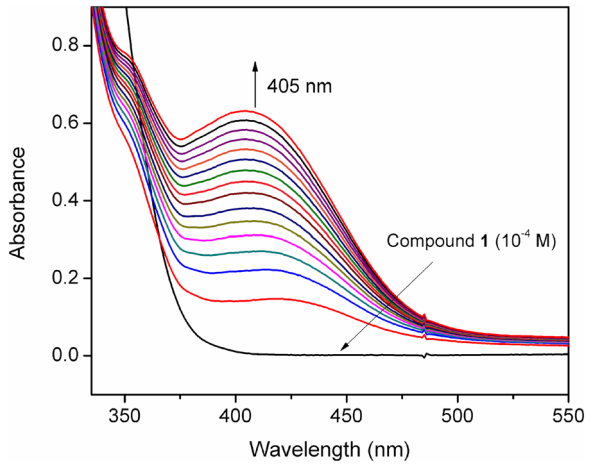

Fig. 4 Increase in the absorbance band at 405 nm upon the addition of 100 equivalents of 3,5-DTBC to a 10^{-4} M oxygen-saturated methanolic solution of **1**.

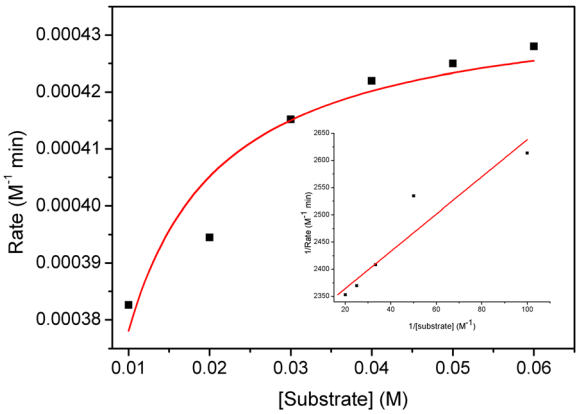

Fig. 5 Plot of initial rates *versus* substrate concentration from the oxidation of 3,5-DTBC catalyzed by **1**. The inset shows the Lineweaver–Burk plot.

Table 2 Kinetic parameters for the oxidation of 3,5-DTBC

Compound	V_{max} (M min^{-1})	K_M (M)	K_{cat} (h^{-1})
1	4.364×10^{-4}	1.54×10^{-3}	157.1×10^{2}

Note: standard error for V_{max} (M min^{-1}) = 4.839×10^{-6} and for K_M = 2.622×10^{-4}.

$CDCl_3$. The ^{1}H NMR data of the product shown in Fig S5, ESI† is similar to that reported in the literature for 3,5-DTBQ,[82] thereby confirming the formation of the *o*-quinone derivative in the reaction medium at 405 nm. The kinetics for the oxidation of 3,5-DTBC to 3,5-DTBQ were determined by the initial rate method at room temperature. The concentration of the substrate was varied in the range from 0.001 to 0.006 M in methanolic solution to a total volume of 2 mL. To each of these substrate solutions, 50 μL from the stock solution of the complex was added to make the concentration of the catalyst as 1×10^{-4} M. The dependence of the initial rate on the concentration of the substrate was monitored spectrophotometrically at 405 nm. Moreover, the initial rate method exhibited first-order dependence on the catalyst and exhibited saturation kinetics at higher substrate concentrations. The Michaelis–Menten model was thus applied to analyze the observed rate *vs.* substrate concentration, while the binding constant (K_M), maximum velocity (V_{max}) and turnover number (K_{cat}) were obtained from the Lineweaver–Burk graph of $1/V$ *vs.* 1/[S] shown as an inset in Fig. 5. The kinetic parameters (V_{max}, K_M, and K_{cat}) for compound **1** are presented in Table 2.

The catecholase activity exhibited by compound **1** was compared with that of compounds reported by various groups, as summarized in Table S4 (ESI†). The catalytic efficiency of the present compound was found to be either comparable, higher, or lower than mono- or dinuclear transition metal compounds reported in the literature, especially in methanol solvent. Upon comparing Table 2 with Table S4 (ESI†), it may be stated that compound **1** belongs to a fairly efficient group of catalysts.

The formation of 3,5-DTBQ is associated with the generation of water or hydrogen peroxide as the end product during the oxidation process, as reported for several compounds in the literature.[61] Some reports suggest that the formation of H_2O_2 largely depends on the metal center involved during the oxidation process.[82] Hence, it was essential to know which species are formed during the reaction; hence, we utilized the iodometric method. The oxidation of I^- species to iodine followed by the generation of I^{3-} species is evident in our case from the absorption band obtained near 353 nm from the UV-Vis spectral study (Fig. S6, ESI†).

3.6. Magnetic properties

The temperature (T) dependence of the magnetization (M) in the presence of an applied magnetic field of H = 100 Oe, was measured for compound **1**. The inverse magnetic susceptibility [$\chi(T)$ = M/H] in the temperature range 60–310 K is shown in Fig. 6. These data show a broad hump-like feature below ≈260 K. However, there is no signature for long-range magnetic ordering in compound **1**. We analyzed the $\chi(T)$ data quantitatively. A closer look at the high-temperature data above 260 K shows that the inverse magnetic susceptibility is linear with temperature. We fitted the data with the Curie–Weiss law, $\chi(T) = C/(T - \theta)$ in the high-temperature range (260–310 K), and the fitted line is shown by the solid straight line in Fig. 6a. Here, C is the Curie constant and θ is the Curie–Weiss temperature. From the fitting, we get $C = 1.0145$ cm^3 K mol^{-1} and $\theta = -4.1$ K. The low and negative value of θ indicates weak antiferromagnetic interaction between Ni(II) spins in compound **1**. The effective moment of the compound was calculated from the Curie constant obtained from the fitting according to the formula:

$$\mu_{eff} = \sqrt{(3k_B C/N_A)},$$

where k_B is the Boltzmann constant and N_A is the Avogadro number. We got $\mu_{eff} \approx 2.85\ \mu_B/Ni^{2+}$, which is very close to the expected spin-only moment of Ni^{2+} ($S = 1$), 2.83 μ_B. Concerning to the analysis of the T-dependence of susceptibility, the Curie–Weiss

law works well in the high-temperature range, but fails to reproduce the hump-like nature below 260 K. This broad hump-like signature represents the existence of short-range magnetic ordering in the system. From the crystal structure of compound **1**, it is pertinent that Ni forms the dinuclear part. Hence, a dimer model is one of the possibilities for modelling the magnetic properties of this compound. We can consider this system as an isolated $S = 1$ dimer. Hence, we can write down the Heisenberg interaction as:

$$H = -2JS_1 \cdot S_2$$

where S_1 and S_2 are the spins of two Ni^{2+} in the Ni-dimer and J is the exchange interaction between them.[83] Now, we can write down the temperature-dependent magnetic susceptibility as:

$$\chi(T) = \frac{N_A g^2 \mu_B{}^2}{3k_B T} \frac{\sum_{S=0}^{2} S(S+1)(2S+1)\exp\left(-\frac{E}{k_B T}\right)}{\sum_{S=0}^{2}(2S+1)\exp\left(-\frac{E}{k_B T}\right)} + \chi_0$$

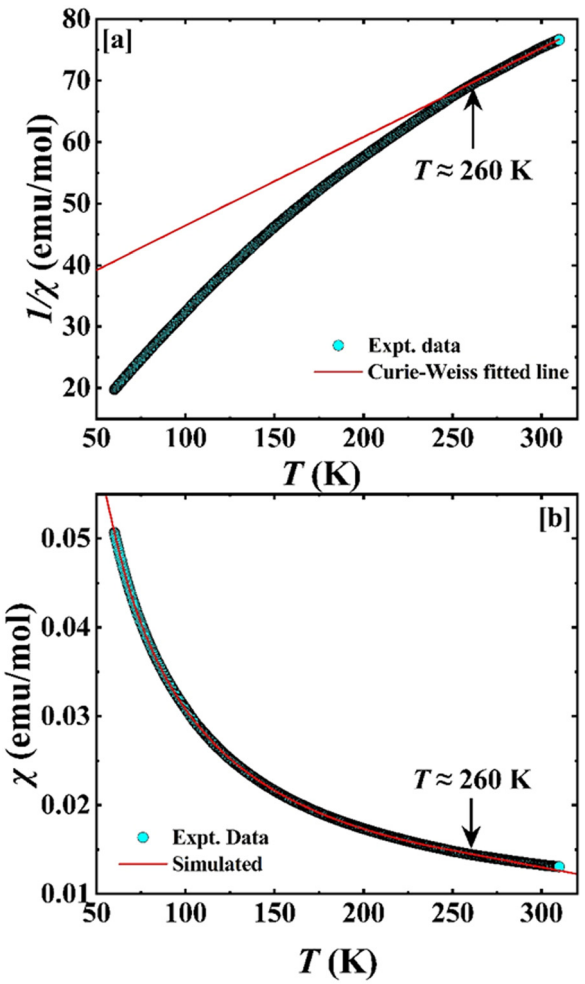

Fig. 6 (a) Temperature-dependent inverse magnetic susceptibility. Scattered points represent the experimental data, while the red solid line is obtained from Curie–Weiss fitting. (b) The $\chi(T)$ data along with the simulated pattern using the isolated dimer model.

where χ_0 is the Curie contribution, g is the Lande-g factor (we consider here the standard value of $g = 2$) and we can write down the energy. Inserting the value of energy for a spin 1 dimer, we can rewrite the above equation as:

$$\chi(T) = \frac{N_A g^2 \mu_B{}^2}{3k_B T} \frac{\sum_{S=0}^{2}\left[6\exp\left(-\frac{2J}{k_B T}\right) + 30\exp\left(-\frac{6J}{k_B T}\right)\right]}{1 + 3\exp\left(-\frac{2J}{k_B T}\right) + 5\exp\left(-\frac{6J}{k_B T}\right)} + \chi_0$$

This equation fits the experimental data satisfactorily, as shown in Fig. 6b. We got $\chi_0 = 2 \times 10^{-5}$ cm^3 mol^{-1} and $J/k_B = 3.08 \pm 0.04365$ K. Therefore, it is evident that Ni(II) forms a dinuclear compound because of isolated dimeric interactions in compound **1**. The major contribution controlling the magnetic coupling (J_{Ni-Ni}) in compound **1** is the phenoxide bridge from *p*-vanillin, which works as a magnetic exchange pathway between the Ni(II) centers.[84,85] From the theoretical and experimental data, the literature discussed in Table S1 (ESI†) suggests that the phenoxide-based Ni–O–Ni angle could be one of the determining factors for the nature of the magnetic interaction shown by compound **1**. It is expected that the phenoxide-bridged dinuclear Ni(II) will show a more negative J_{Ni-Ni} with larger Ni–O–Ni bond angle than 93–96°. In compound **1**, the average Ni–O–Ni bond angle is 93.5°, responsible for feeble antiferromagnetic interactions between the two nickel centers and is in good agreement with the well-established magneto-structural correlation.[86–89]

4. Biological evaluation

4.1. Cytotoxicity studies of 1

Compound **1** showed dose-dependent toxicity toward HepG2 cancer cells, as depicted in Fig. 7a. Compared with *cis*-platin, only 6.67 ± 0.120% cell viability was observed for **1** against HepG2 cell lines at 100 μg mL^{-1}. The growth inhibition effect on HepG2 cell lines increased with an increase in concentration of **1**, with 78.9 ± 0.11% cell viability at 3.12 μg mL^{-1}. Three dicobalt(II) complexes of *p*-cresol-based "end-off" compartmental ligands 2,6-bis(R-iminomethyl)-4-methyl-phenolate, where R = *N*-ethylpiperazine, 2-ethylpyridine or *N*-ethylpiperidine for three different compounds inhibited the proliferation of HepG2 by more than 50% at 100 μM mL^{-1} (~88.86 μg mL^{-1}).[63] However, in the present study, 33.15 μM concentration (~25 μg mL^{-1}) resulted in >50% cell death. In another study by Biswas *et al.*,[90] a new azido-bridged dinuclear copper(II) thiosemicarbazide complex showed cytotoxicity against AGS and A549 cancer cells. The complex showed concentration-dependent cytotoxic activity with >50% killing observed for 0.5 μg mL^{-1} (~0.83 μM mL^{-1}) in both cell lines.

The cytotoxic effect of the synthesized complex on the cancer cell line was also observed using light microscopy (Fig. 7b). The untreated HepG2 cells were highly dense, confluent, and abundant, but treatment with different concentrations of **1** inhibited the proliferation of cells. Additionally, the shrinkage of cells

was observed after circularization, resulting in a decrease in the adherence and density of cells. Similar morphological alterations in the HeLa cervical cell line (spherical and granular changes in shape) have been reported recently in the presence of nickel with the Schiff base vanillin-4-methyl-4-phenyl-3-thiosemicarbazone complex.[91] It was observed that *cis*-platin showed an IC50 value of 2.23 ± 0.02 μg mL^{-1} (2.95 μM mL^{-1}) which is eleven times more effective than **1**, *i.e.* 22.82 ± 0.09 μg mL^{-1} (30.26 μM mL^{-1}), on HepG2 cancerous cells. However, an IC50 value of 54.3 ± 1.7 μg mL^{-1} was observed against HeLa cervical cell lines by a complex of nickel with Schiff base vanillin-4-methyl-4-phenyl-3-thiosemicarbazone.[91] In contrast, IC50 of 4.3 μM and 10 μM were observed for an azido-bridged dinuclear copper(II) thiosemicarbazide complex against AGS and A549 cancer cells, respectively.[90] Although compound **1** has a high IC50 value, it is apparent that the complex can inhibit the proliferation of HepG2 cells in a dose-dependent manner, indicating that this complex can be used as an effective agent for antitumor activity. The individual action of free ligand and $Ni(OAc)_2$ can be ruled out according to an earlier report for the [Cu(phen)$(van)_2$] complex. The authors observed individual properties of vanillin, phenanthroline, and $CuCl_2$ above 150 mmol mL^{-1}, indicating the non-cytotoxic effect of these isolated species. The activity of **1** in cancer cells may be due to the generation of reactive oxygen species (ROS) through the transfer of electrons from metal ions to oxygen, resulting in cell death.[65] Generally, the metal complexes of copper, cobalt, zinc, and nickel with various ligands, and specifically vanillin complexes with these metals have been reported for their cytotoxicity against various cancer cell lines, such as B16–F10, HUH-7, 786-0, MCF-7, MDA-MB-231, A375, LNcaP, HK-2, HepG2 and HeLa.[63,66,90,92–96] However, a recent study has highlighted the applicability of nickel(II) complexes derived from vanillin with much higher anticancer activities than other metal complexes, indicating that the anticancer potency is also metal-dependent.[97] In another study, the low cytotoxicity of ligands (L1, benzyl 2-(cyclobutanylidene)hydrazinecarboxylate; L2, benzyl 2-(cyclopentanylidene)hydrazinecarboxylate; L3, benzyl 2- (cyclohexanylidene)hydrazinecarboxylate and ammonium thiocyanate) and nitrate salts of Co(II) or Ni(II) used to form a series of mononuclear cobalt and nickel complexes were reported.[98] Similarly, Liu *et al.*[99] documented the low cytotoxicity and absence of DNA cleavage activity for free ligand (H-ClQ) and $NiCl_2$ used for the preparation of a dinuclear Ni(II) complex with 5,7-dichloro-8-hydroxyl quinolone (H-ClQ).

4.2. DNA cleavage activity

The direct activity of compound **1** on DNA cleavage was determined by the formation of a relaxed or nicked circular form (form II) due to a single-strand break or by a linear form (form III) *via* a double-strand break from circular supercoiled plasmid DNA (form I). This study is important since DNA is reported to be a specific target for metal complexes of transition elements such as cobalt[63] and copper,[65] exhibiting potential antitumor properties. Fig. 8 shows the differential electrophoreses pattern for DNA cleavage after interacting with **1**. From the assay, it is clear that **1** showed a dose-dependent rise in forms II and III. It was observed that, at 80 μM concentration, DNA cleavage is very prominent with diffused form I compared to 10, 20, and 40 μM concentrations. However, decreases in the fluorescence intensity of supercoiled (SC) (form I), nicked circular (NC) (form II), and linear (L) (form III) forms were observed for all complex concentrations tested for DNA cleavage activity, while no DNA cleavage activity was observed for the control. In the case of the [Cu(phen)$(van)_2$] complex, maximum DNA cleavage activity was observed in the presence of hydrogen peroxide initiated at 10 μM, resulting in the formation of relaxed (form II) and linear (form III) DNA compared to only the relaxed (form II) in the presence of glutathione.[65] The authors also confirmed the improved DNA cleavage activity due to the vanillin ligand compared to its precursor complex [Cu(phen)Cl_2]. In another study, dicobalt(II) complexes of *p*-cresol-based ligands have been reported to cleave DNA prominently at a concentration above 100 μM, exhibiting the form II of DNA.[63] The mechanism of pBR322 cleavage in this study can be explained by hydrolytic cleavage and the generation of free radicals by compound **1** at various concentrations, as observed for vanillin or polypyridyl or

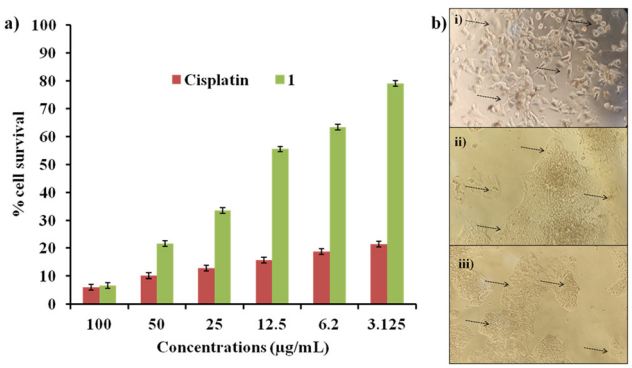

Fig. 7 Cytotoxicity studies of compound **1** against HepG2 cancerous cells determined using an MTT assay. (a) Percentage cell survival of HepG2 cancerous cells *via* the dose-dependent anti-proliferative activity of **1**. (b) Microscopic images of HepG2 cells: control cells without **1** (i), cells treated with 3.25 μg mL^{-1} of **1** (ii), and cells treated with 12.5 μg mL^{-1} of **1**.

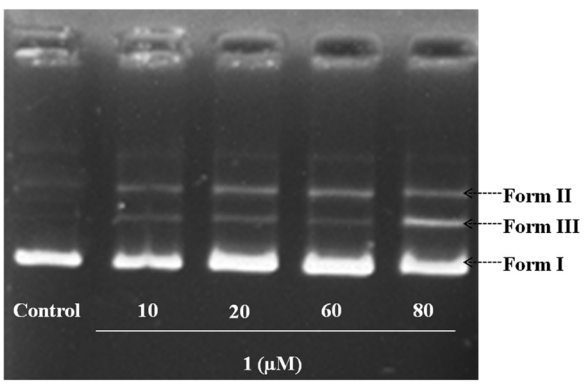

Fig. 8 DNA cleavage assay employing plasmid DNA pBR322 with **1** at different concentrations (10, 20, 60, and 80 μM).

N-ethylpiperazine, 2-ethylpyridine, and *N*-ethylpiperidine based metal complexes.[63,66,100,101]

5. Conclusions

A new dinuclear nickel(II) compound **1** bearing vanillin, acetate, isothiocyanate, and aqua ligands has been synthesized. Acetatato ligands act as the capping agent binding the two nickel(II) ions through *syn–syn* coordination mode, while the *p*-vanillin exhibits bridging through the phenolic oxygen contributing towards magnetic interactions. Compound **1** showed weak antiferromagnetic interaction, indicated by the low θ value (−4.1 K), obtained by fitting the magnetic data with the Curie–Weiss law. Compound **1** exhibits catecholase activity in the oxidation of 3,5-di-*tert*-butylcatechol to corresponding quinone with K_{cat} = 157.1 × 10^2 h^{-1}. Compound **1** also exhibited potent cytotoxicity and DNA cleavage in biological activity studies.

Conflicts of interest

The authors declare that they have no known competing financial interests or personal relationships that could have appeared to influence the work reported in this paper.

Acknowledgements

Authors acknowledge the financial support to School of Chemical Sciences, Goa University by DST, New Delhi under DST-FIST Scheme (No. SR/FST/CSII-034/2014(C) and UGC, New Delhi under SAP programme (No. F.504/14/DSA-I/2015). Beena K. Vernekar thanks the Directorate of Higher Education, Government of Goa for the grant of sabbatical leave and the Dean, School of Chemical Sciences, Goa University for laboratory facilities during the leave. Beena K. Vernekar also acknowledge DST-Goa for the sanction of project (grant no. 6-331-2018/S&T-DIR/302). Nikita N. Harmalkar acknowledge UGC for the Savitribai Jyotirao Phule Fellowship for Single Girl Child (SJSGC) [UGCES-22-OB-GOA-F-SJSGC-6907]. JS thank SERB, DST-India for the Ramanujan Fellowship [RJF/2019/000046 (SQUID-1986-JS-3632)]. Authors acknowledge ACMS, IIT, Kanpur, CSIF, BITS Goa campus and Central Instrumentation Facility, IISER, Bhopal for XPS, PXRD and SQUID facilities, respectively. Authors acknowledge the Maratha Mandal's Central Research Laboratory, Belgavi, Karnataka for DNA cleavage and cytotoxicity studies. Authors thank Dr Venkatesha R. Hathwar, School of Physical and Applied Sciences, Goa University for the valuable discussions on crystal structure of **1** and refinement of data.

References

1 N. E. Dixon, C. Gazzola, R. L. Blakeley and B. Zerner, *J. Am. Chem. Soc.*, 1975, **97**, 4131–4133.
2 R. K. Watt and P. W. Ludden, *Cell. Mol. Life Sci.*, 1999, **56**, 604–625.
3 H. L. Mobley and R. P. Hausinger, *Microbiol. Rev.*, 1989, **53**, 85–108.
4 *Comprehensive Coordination Chemistry II*, ed. F. Meyer, H. Kozlowski, J. A. M. Cleverty, and T. J. Meyer, Elsevier, 2003, pp. 247–554.
5 H. Youn, E. Kim, J. Roe, Y. Hah and S. Kang, *J. Biochem.*, 1996, **318**, 889–896.
6 R. K. Andrews, R. L. Blakeley and B. Zerner, in H. Sigel, A. Sigel Marcel Dekker Inc., New York, 1988, **23**, 165–284.
7 M. Can, F. A. Armstrong and S. W. Ragsdale, *Chem. Rev.*, 2014, **114**, 4149–4174.
8 S. Friedle, E. Reisner and S. Lippard, *J. Chem. Soc. Rev.*, 2010, **39**, 2768–2779.
9 P. C. A. Bruijnincx, G. van. Koten and G. R. J. M. Klein, *Chem. Soc. Rev.*, 2008, **37**, 2716–2744.
10 S. I. Chan and S. S.-F. Yu, *Acc. Chem. Res.*, 2008, **41**, 969–979.
11 R. Hage and A. Lienke, *Angew. Chem.*, 2006, **118**, 212–229.
12 N. Duran and E. Esposito, *Appl. Catal., B*, 2000, **28**, 83–99.
13 L. Que and W. B. Tolman, *Nature*, 2008, **455**, 333–340.
14 M. Saito, R. Arakaki, A. Yamada, T. Tsunematsu, Y. Kudo and N. Ishimaru, *Int J. Mol Sci.*, 2016, **17**, 202.
15 C. Hsu, C. Kuo, S. Chuang and M. Hou, *Biometals*, 2013, **26**, 1–12.
16 G. Morgant, N. Bouhmaida, L. Balde, N. E. Ghermani and J. d'Angelo, *Polyhedron*, 2006, **25**, 2229–2235.
17 P. Bombicz, E. Forizs, J. Madarasz, A. Deak and A. Kalman, *Inorg. Chim. Acta*, 2001, **315**, 229–235.
18 O. Z. Yesilel, M. S. Soylu, H. Olmez and O. Buyukgungor, *Polyhedron*, 2006, **25**, 2985–2992.
19 K. C. Skyrianou, E. K. Efthimiadou, V. Psycharis, A. Terzis, D. P. Kessissoglou and G. Psomas, *J. Inorg. Biochem.*, 2009, **103**, 1617.
20 B. Xu, P. Shi, Q. Guan, X. Shi and G. Zhao, *J. Coord. Chem.*, 2013, **66**, 2605–2614.
21 K. Alomar, A. Landreau, M. Allain, G. Bouet and G. Larcher, *J. Inorg. Biochem.*, 2013, **126**, 76–83.
22 H. B. Shawish, W. Wong, Y. Wong, S. Loh, C. Looi, P. Hassandarvish, A. Phan, W. Wong, H. Wang, I. C. Paterson, C. Ea, M. Mustafa and M. J. Maah, *PLoS One*, 2014, **9**, e100933.
23 K. C. Skyrianou, F. Perdih, A. N. Papadopoulos, I. Turel, D. P. Kessissoglou and G. Psomas, *J. Inorg. Biochem.*, 2011, **105**, 1273–1285.
24 P. Sathyadevi, P. Krishnamoorthy, E. Jayanthi, R. R. Butorac, A. H. Cowley and N. Dharmaraj, *Inorg. Chim. Acta*, 2012, **384**, 83–96.
25 Y. Li, Z. Yang and J. Wu, *Eur. J. Med. Chem.*, 2010, **45**, 5692–5701.
26 R. Prabu, A. Vijayaraj, R. Suresh, R. Senbhagaraman, V. Kaviyarasan and V. Narayanan, *J. Coord. Chem.*, 2013, **66**, 206–217.
27 F. Bisceglie, S. Pinelli, R. Alinovi, M. Goldoni, A. Mutti, A. Camerini, L. Piola, P. Tarasconi and G. Pelosi, *J. Inorg. Biochem.*, 2014, **140**, 111–125.

28 G. Barone, N. Gambino, A. Ruggirello, A. Silvestri, A. Terenzi and V. T. Liveri, *J. Inorg. Biochem.*, 2009, **103**, 731–737.
29 P. J. Cox, G. Psomas and C. A. Bolos, *Bioorg. Med. Chem.*, 2009, **17**, 6054–6062.
30 S. Betanzos-Lara, C. Gómez-Ruiz, L. R. Barrón-Sosa, I. Gracia-Mora, M. Flores-Álamo and N. Barba-Behrens, *J. Inorg. Biochem.*, 2012, **114**, 82–93.
31 X. Totta, A. A. Papadopoulou, A. G. Hatzidimitriou, A. Papadopoulos and G. Psomas, *J. Inorg. Biochem.*, 2015, **145**, 79–93.
32 Z. Afrasiabi, E. Sinn, W. Lin, Y. Ma, C. Campana and S. Padhye, *J. Inorg. Biochem.*, 2005, **99**, 1526.
33 G. Blondin and J. J. Girerd, *Chem. Rev.*, 1990, **90**, 1359–1376.
34 P. Amo-Ochoa, O. Castillo, P. J. S. Miguel and F. Zamora, *J. Inorg. Biochem.*, 2008, **102**, 203–208.
35 M. Wenzel, A. de Almeida, E. Bigaeva, P. Kavanagh, M. Picquet, P. L. Gendre, E. Bodio and A. Casini, *Inorg. Chem.*, 2016, **55**, 2544–2557.
36 I. K. Pandey, M. Natarajan and S. Kaur-Ghumaan, *J. Inorg. Biochem.*, 2015, **143**, 88–110.
37 I. Almendras, Y. Huentupil, N. Novoa, P. Roussel, D. R. Melis, G. S. Smith and R. Arancibia, *Inorg. Chim. Acta*, 2019, **496**, 119050.
38 T. Hamaguchi, R. Shimazaki and I. Ando, *J. Mol. Struct.*, 2018, **1173**, 345–348.
39 D. Volkmer, B. Hommerich, K. Griesar, W. Haase and B. Krebs, *Inorg. Chem.*, 1996, **35**, 3795.
40 S. Thalamuthu and M. A. Neelakantan, *Inorg. Chim. Acta*, 2021, **516**, 120109.
41 I. P. Kalatuwawege, M. J. Gunaratna and D. N. Udukala, *Molecules*, 2021, **26**, 6658.
42 A. Guha, K. S. Banu, S. Das, T. Chattopadhyay, R. Sanyal, E. Zangrando and D. Das, *Polyhedron*, 2013, **52**, 669–678.
43 A. Biswas, L. K. Das, M. G. Drew, G. Aromí, P. Gamez and A. Ghosh, *Inorg. Chem.*, 2012, **51**, 7993–8001.
44 S. Majumder, S. Mondal, P. Lemoineb and S. Mohanta, *Dalton Trans.*, 2013, **42**, 4561–4569.
45 K. S. Bharathi, S. Sreedaran, A. K. Rahman, K. Rajesh and N. Narayanan, *Polyhedron*, 2007, **26**, 3993–4002.
46 T. Chattopadhyay, M. Mukherjee, A. Mondal, P. Maiti, A. Banerjee, K. S. Banu Bhattacharya, S. B. Roy, D. J. Chattopadhyay, T. K. Mondal, M. Nethaji, E. Zangrando and D. Das, *Inorg. Chem.*, 2010, **49**, 3121–3129.
47 M. B. Hocking, *J. Chem. Edu.*, 1997, **74**, 1055–1059.
48 C. Andraud, T. Brotin, C. Garcia, F. Pellé, P. Goldner, B. Bigot and A. Collet, *J. Am. Chem. Soc.*, 1994, **116**, 2094–2102.
49 S. Radhakrishnan, D. Jayaram and D. Anduselvi, *Int. J. Chem. Tech. Res.*, 2013, **5**, 2717–2726.
50 D. T. Shaughnessy, R. W. Setzer and D. M. De Marini, *Mutat. Res.*, 2001, **480–481**, 55–69.
51 H. Imanishi, Y. F. Sasaki, K. Matsumoto, M. Watanabe, T. Ohta, Y. Shirasu and K. Tutikawa, *Mutat. Res. Lett.*, 1990, **243**, 151–158.
52 B. K. Vernekar, G. Kotkar, L. R. D'souza, V. R. Hathwar and S. N. Dhuri, *J. Mol. Struct.*, 2023, **1295**, 136537.
53 D.-D. Lin and D. J. Xu, *Acta Cryst.*, 2005, 1821–1822.
54 B. Kozlevčar, B. Mušič, N. Lah, I. Leban and P. Šegedin, *Acta Chim. Slov.*, 2005, **52**, 40–43.
55 S. C. Kumar, A. K. Ghosh, J.-D. Chen and R. Ghosh, *Inorg. Chim. Acta*, 2017, **464**, 49–54.
56 Y. H. Fan, Y. N. Zou, C. F. Bi, A. D. Wang and F. Guo Koord Khim, *Coord. Chem.*, 2007, **33**, 582.
57 C.-L. Lan, S.-H. Zhang, F. Zhong and Y.-M. Jiang, Guangxi Shifan Daxue Xuebao Ziran Kexueban(Chin.)(J. Guangxi Normal University), 2002, **20**, 52.
58 G. Sheldrick, *Acta. Cryst.*, 2015, **C71**, 3–8.
59 S. Mondal, B. Pakhira, A. J. Blake, M. G. B. Drew and S. K. Chattopadhyay, *Polyhedron*, 2016, **117**, 327–337.
60 J. L. Viegas and S. N. Dhuri, *J. Mol. Struct.*, 2023, **1288**, 135719.
61 J. Adhikary, P. Chakraborty, S. Das, T. Chattopadhyay, A. Bauza, S. K. Chattopadhyay, B. Ghosh, F. A. Mautner, A. Frontera and D. Das, *Inorg. Chem.*, 2013, **52**, 13442–13452.
62 A. Neves, L. M. Rossi, A. J. Bortoluzzi, B. Szpoganicz, C. Wiezbicki and E. Schwingel, *Inorg. Chem.*, 2002, **41**, 1788–1794.
63 A. Banerjee, A. Guha, J. Adhikary, A. Khan, K. Manna, S. Dey and D. Das, *Polyhedron*, 2013, **60**, 102–109.
64 M. N. Ahamad, M. Kumar, A. Ansari, I. Mantasha, M. Ahmad and M. Shahid, *New J. Chem.*, 2019, **43**, 14074–14083.
65 W. M. T. Q. de Medeiros, M. J. C. de Medeiros, E. M. Carvalho, J. A. de Lima, V. da Oliveira, A. C. F. de Pontes, F. O. N. da Silva, J. A. Ellena, H. A. de Rocha, E. H. S. de Sousa and D. de Pontes, *RSC Adv.*, 2018, **8**, 16873–16886.
66 K. Nakamoto, *Infrared and Raman Spectra of Inorganic and Coordination Compounds part B: applications in coordination, organometallic, and bioinorganic chemistry*, John Wiley, 6th edn, 2009, pp. 149–354.
67 Z. Nickolov, G. Georgiev, D. Stoilova and I. Ivanov, *J. Mol. Struct.*, 1995, **354**, 119–125.
68 F. Rhoufal, N. Sergent, A. Laachir, S. Obbade, S. Guesmi, M. Akkurt, L. Jouffret and F. Bentis, *Chem. Select*, 2019, **4**, 7773–7783.
69 S. K. Tadavi, A. A. Yadav and R. S. Bendre, *J. Mol. Struct.*, 2018, **1152**, 223–231.
70 P. Mukherjee, C. Biswas, M. G. B. Drew and A. Ghosh, *Polyhedron*, 2007, **26**, 3121–3128.
71 M. Đaković, Z. Popović and N. Smrečki-Lolić, *J. Mol. Struct.*, 2008, **888**, 394–400.
72 P. Nithya, S. Helena, J. Simpson, M. Ilanchelian, A. Muthusankar and S. Govindarajan, *J. Photochem. Photobiol. B. Biol.*, 2016, **165**, 220–231.
73 A. Sasmal, E. Garribba, V. Ugone, C. Rizzoli and S. Mitra, *Polyhedron*, 2017, **121**, 107–114.
74 S. S. Massoud, C. C. Ledet, T. Junk, S. Bosch, P. Comba, R. Herchel, J. Hošek, Z. Trávníček, R. C. Fischer and F. A. Mautner, *Dalton Trans.*, 2016, **45**, 12933–12950.
75 P. Nithya, J. Simpson and S. Govindarajan, *Polyhedron*, 2018, **141**, 5–16.
76 A. Fereday, D. M. L. Goodgame, P. D. Lickiss, S. J. Rooke, A. J. P. White and D. J. Williams, *Inorg. Chem. Commun.*, 2002, **5**, 805–807.

77 F. A. Mautner, R. C. Fischer, L. G. Rashmawi, F. R. Louka and S. S. Massoud, *Polyhedron*, 2017, **124**, 237–242.
78 A. Majumder, G. M. Rosair, A. Mallick, N. Chattopadhyay and S. Mitra, *Polyhedron*, 2006, **25**, 1753–1762.
79 M. Jafari, M. Salehi, M. Kubicki and A. Khaleghian, *Russ. J. Coord. Chem.*, 2018, **44**, 21–31.
80 A. Sarkar, A. Chakraborty, A. Adhikary, S. Maity, A. Mandal, D. Samanta, P. Ghosh and D. Das, *Dalton Trans.*, 2019, **48**, 14164–14177.
81 A. Pal, S. C. Kumar, A. K. Ghosh, C.-H. Lin, E. Rivière, T. Mallah and R. Ghosh, *Polyhedron*, 2016, **110**, 221–226.
82 S. K. Dey and A. Mukherjee, *J. Mol. Catal. A: Chem.*, 2015, **407**, 93–101.
83 P. Khuntia and A. V. Mahajan, *J. Phys.: Condens. Matter*, 2010, **22**, 296002.
84 K. K. Nanda, R. Das, L. K. Thompson, K. Venkatsubramanian, P. Paul and K. Nag, *Inorg. Chem.*, 1994, **33**, 1188–1193.
85 A. Paul, A. Figuerola, H. Puschmann and S. C. Manna, *Polyhedron*, 2019, **157**, 39–48.
86 A. Burkhardt, E. T. Spielberg, S. Simon, H. Gçrls, A. Buchholz and W. Plass, *Chem. – Eur. J.*, 2009, **15**, 1261–1271.
87 X.-H. Bu, M. Du, L. Zhang, D.-Z. Liao, J.-K. Tang, R.-H. Zhang and M. Shionoya, *J. Chem. Soc., Dalton Trans.*, 2001, 593–598.
88 R. Biswas, S. Giri, S. K. Saha and A. Ghosh, *Eur. J. Inorg. Chem.*, 2012, 2916–2927.
89 S. Dasgupta, J. Adhikary, S. Giri, A. Bauza, A. Frontera and D. Das, *Dalton Trans.*, 2017, **46**, 5888–5900.
90 N. Biswas, S. Khanra, A. Sarkar, S. Bhattacharjee, D. P. Mandal, A. Chaudhuri and C. R. Choudhury, *New J. Chem.*, 2017, **41**, 12996–13011.
91 L. V. Kumar, S. Sunitha and G. R. Nath, *Mater. Today: Proc.*, 2021, **41**, 669–675.
92 P. Nagababu, A. K. Barui, B. Thulasiram, C. S. Devi, S. Satyanarayana, C. R. Patra and B. Sreedhar, *J. Med. Chem.*, 2015, **58**, 5226–5241.
93 S. Kathiresan, S. Mugesh, M. Murugan, F. Ahamed and J. Annara, *RSC Adv.*, 2016, **6**, 1810–1825.
94 Z. F. Chen, M. X. Tan, L. M. Liu, Y. C. Liu, H. S. Wang, B. Yang and C. Orvig, *Dalton Trans.*, 2009, 10824–10833.
95 A. Hassan and A. Said, *Adv. J. Chem., Sect. A*, 2020, **4**, 87–103.
96 L. Zarei, Z. Asadi, M. Dusek and V. Eigner, *J. Photochem. Photobio. A: Chem.*, 2019, **374**, 145–160.
97 H. Bahron, S. S. Khaidir, A. M. Tajuddin, K. Ramasamy and B. M. Yamin, *Polyhedron*, 2019, **161**, 84–92.
98 P. Nithya, R. Rajamanikandan, J. Simpson, M. Ilanchelian and S. Govindarajan, *Polyhedron*, 2018, **145**, 200–217.
99 Y. C. Liu, X. Y. Song, Z. F. Chen, Y. Q. Gu, Y. Peng and H. Liang, *Inorg. Chim. Acta*, 2012, **382**, 52–58.
100 X. F. Zhao, Y. Ouyang, Y. Z. Liu, Q. J. Su, H. Tian, C. Z. Xie and J. Y. Xu, *New J. Chem.*, 2014, **38**, 955–965.
101 M. Salimi, K. Abdi, H. M. Kandelous, H. Hadadzadeh, K. Azadmanesh, A. Amanzadeh and H. Sanati, *Biometals*, 2015, **28**, 267–278.